Band Electronic Structure of the Purple Potassium Molybdenum Bronze $K_{0.9}Mo_6O_{17}$

Myung-Hwan Whangbo,*[1a] Enric Canadell,[1b] and Claire Schlenker[1c]

Contribution from the Department of Chemistry, North Carolina State University, Raleigh, North Carolina 27695-8204, Laboratoire de Chimie Théorique, Université de Paris-Sud, 91405 Orsay Cedex, France, and Laboratoire d'Études des Propriétés Électroniques des Solides, CNRS, 38042 Grenoble Cedex, France. *Received February 9, 1987*

Abstract: The electronic properties of potassium molybdenum purple bronze $K_{0.9}Mo_6O_{17}$ were examined by performing tight-binding band calculations on a single Mo_6O_{17} layer. Our calculations show the presence of three partially filled d-block bands, which are essentially derived from the t_{2g} orbitals of the MoO_6 octahedra belonging to the innermost two sublayers of Mo_6O_{17}. The Fermi surfaces of the three partially filled bands are all closed, and thus $K_{0.9}Mo_6O_{17}$ is a two-dimensional metal. The charge density wave of $K_{0.9}Mo_6O_{17}$, which sets in at 120 K, is caused by the nesting of one of the three Fermi surfaces, and the remaining two provide electron and hole carriers below 120 K. The t_{2g}-block bands of the innermost two sublayers of Mo_6O_{17} were examined by analyzing the band orbitals at a few high-symmetry wave vector points. The dispersion characteristics of those bands are determined by whether or not the orbitals of bridging oxygen atoms can mix with the molybdenum t_{2g} orbitals.

Molybdenum bronzes are a class of solid oxide phases with a range of composition $A_xMo_yO_z$, where A is an alkali metal or Tl,[2] and exhibit intense color. There are three well-defined molybdenum bronzes: The red bronze $A_{0.33}MoO_3$ (A = K)[3,4] and the blue bronze $A_{0.3}MoO_3$ (A = K, Rb, Tl)[3,5,6] contain separated metal–oxygen layers of composition MoO_3 that are constructed from MoO_6 octahedra. The potassium purple bronze $K_{0.9}Mo_6O_{17}$[7-9] has separated metal–oxygen layers of composition Mo_6O_{17}, which are made up of both MoO_6 octahedra and MoO_4 tetrahedra. The sodium purple bronze $Na_{0.9}Mo_6O_{17}$[10] and the thallium purple bronze $TlMo_6O_{17}$[11] are similar in structure to the potassium purple bronze, but the lithium purple bronze $Li_{0.9}Mo_6O_{17}$[12] differs from the other purple bronzes in that it has no separated metal–oxygen layers.[12a]

An alkali metal atom of a bronze $A_xMo_yO_z$ donates its valence electron to the d-block bands of the transition metal Mo, so the nature of these bands determines whether the bronze is a metal or an insulator. The red bronze $A_{0.33}MoO_3$ is a semiconductor at all temperatures,[4b] while the blue bronze $A_{0.3}MoO_3$ is a quasi-one-dimensional (1D) metal above 180 K, below which it becomes a semiconductor due to a charge density wave (CDW) formation.[6] This difference in the electrical properties of the two bronzes originates from the fact that their MoO_3 layers do not have identical structures.

The potassium purple bronze $K_{0.9}Mo_6O_{17}$ is a two-dimensional (2D) metal above 120 K, at which it undergoes a CDW phase transition.[8,9] In contrast to the case of the blue bronze, however, the potassium purple bronze remains a 2D metal after the CDW phase transition.[8] Diffuse X-ray scattering and electron diffraction studies show the occurrence of superlattice spots at $q_a = (a^*/2, 0, 0)$, $q_b = (0, b^*/2, 0)$, and $q_{a+b} = (a^*/2, b^*/2, 0)$ below 120 K.[9b] That is, the CDW formation increases the unit cell dimension fourfold, from (a, b, c) to $(2a, 2b, c)$. The CDW vectors q_a, q_b, and q_{a+b} are commensurate within 4% experimental accuracy.[9b] According to the thermoelectric power measurements, the major carriers for electrical transport in $K_{0.9}Mo_6O_{17}$ are electrons and holes above and below 120 K, respectively, and the CDW removes not all but about 50% of the carrier concentration.[8a] Hall effect measurements show the presence of both electrons and holes below 120 K. According to these observations, several partially filled d-block bands are present in $K_{0.9}Mo_6O_{17}$. In electrical, CDW, and other physical properties, $Na_{0.9}Mo_6O_{17}$[10] and $TlMo_6O_{17}$[11] are similar to $K_{0.9}Mo_6O_{17}$.

In understanding the properties of the potassium, sodium, and thallium molybdenum purple bronzes, it is crucial to know their band electronic structures. In the present study, we report our tight-binding band calculations on $K_{0.9}Mo_6O_{17}$ based upon the extended-Hückel method.[13] The results of our band calculations on $K_{0.9}Mo_6O_{17}$ should also be valid for $Na_{0.9}Mo_6O_{17}$ and $TlMo_6O_{17}$. It is noted that similar band calculations performed on the blue bronze[6f] led to results in excellent agreement with experiment. The atomic parameters employed in the present work

(1) (a) North Carolina State University. (b) Laboratoire de Chimie Théorique, Université de Paris-Sud. (c) Laboratoire d'Études des Propriétés Électroniques des Solides.

(2) (a) Sienko, M. J. *Nonstoichiometric Compounds*; Gould, R. F., Ed.; American Chemical Society: Washington, DC, 1963; p 224. (b) Hagenmuller, P. *Prog. Solid State Chem.* **1971**, *5*, 71. (c) Wells, A. F. *Structural Inorganic Chemistry*, 5th ed.; Clarendon: Oxford, 1984; p 612. (d) Schlenker, C.; Dumas, J.; Escribe-Filippini, C.; Guyot, H.; Marcus, J.; Fourcaudot, G. *Philos. Mag. B* **1985**, *52*, 643.

(3) Wold, A.; Kunnmann, W.; Arnott, R. J.; Ferretti, A. *Inorg. Chem.* **1964**, *3*, 345.

(4) (a) Stephenson, N. C.; Wadsley, A. D. *Acta Crystallogr.* **1965**, *18*, 241. (b) Bouchard, G. H.; Perlstein, J. H.; Sienko, M. J. *Inorg. Chem.* **1967**, *6*, 1682.

(5) (a) Graham, J.; Wadsley, A. D. *Acta Crystallogr.* **1966**, *20*, 93. (b) Ghedira, M.; Chenavas, J.; Marezio, M.; Marcus, J. *J. Solid State Chem.* **1985**, *57*, 300. (c) Ganne, M.; Boumaza, A.; Dion, M.; Dumas, J. *Mater. Res. Bull.* **1985**, *20*, 1297.

(6) (a) Schlenker, C.; Dumas, J. *Crystal Structures and Properties of Materials with Quasi One-Dimensional Structures*; Rouxel, J., Ed.; Reidel: Dordrecht, The Netherlands, 1986; p 135. (b) Pouget, J. P.; Noguerra, C.; Moudden, A. H.; Moret, T. *J. Phys. (Les Ulis, Fr.)* **1985**, *46*, 1731. (c) Pouget, J. P.; Kagoshima, S.; Schlenker, C.; Marcus, J. *J. Phys. Lett.* **1983**, *44*, L113. (d) Fleming, R. M.; Schneemeyer, L. F.; Moncton, D. E. *Phys. Rev. B: Condens. Matter* **1985**, *31*, 899. (e) Sato, M.; Fujishita, H.; Hoshino, S. *J. Phys. C* **1985**, *18*, 2603. (f) Whangbo, M.-H.; Schneemeyer, L. F. *Inorg. Chem.* **1986**, *25*, 2424.

(7) Vincent, H.; Ghedira, M.; Marcus, J.; Mercier, J.; Schlenker, C. *J. Solid State Chem.* **1983**, *47*, 113.

(8) (a) Buder, R.; Devenyi, J.; Dumas, J.; Marcus, J.; Mercier, J.; Schlenker, C. *J. Phys. (Les Ulis, Fr.)* **1982**, *43*, L59. (b) Bervas, E.; Cochrane, R. W.; Dumas, J.; Escribe-Filippini, C.; Marcus, J.; Schlenker, C. *Lect. Notes Phys.* **1985**, 217.

(9) (a) Dumas, J.; Bervas, E.; Marcus, J.; Salomon, D.; Schlenker, C. *J. Magn. Magn. Mater.* **1983**, *31-34*, 535. (b) Escribe-Filippini, C.; Konate, K.; Marcus, J.; Schlenker, C.; Almairac, R.; Ayroles, R.; Roucau, C. *Philos. Mag. B* **1984**, *50*, 321.

(10) (a) Gatehouse, B. M.; Lloyd, D. J.; Miskin, B. K. *NBS Spec. Publ. (U.S.)* **1972**, *No. 364*, 15. (b) Stephenson, N. C. *Acta Crystallogr.* **1966**, *20*, 59. (c) Greenblatt, M.; Ramanujachary, K. V.; McCaroll, W. H.; Neifeld, R.; Waszczak, J. V. *J. Solid State Chem.* **1985**, *59*, 149.

(11) (a) Ganne, M.; Dion, M.; Bouzama, A.; Tournoux, M. *Solid State Commun.* **1986**, *59*, 137. (b) Ramanujachary, K. V.; Collins, B. T.; Greenblatt, M. *Solid State Commun.* **1986**, *59*, 647.

(12) (a) Onoda, M.; Toriumi, K.; Matsuda, Y.; Sato, M. *J. Solid State Chem.*, in press. (b) Schlenker, C.; Schwenk, H.; Escribe-Filippini, C.; Marcus, J. *Physica B+C*: **1985**, *135B+C*, 511. (c) Greenblatt, M.; McCaroll, W. H.; Neifeld, R.; Croft, M.; Waszczak, J. V. *Solid State Commun.* **1984**, *51*, 671. (d) Ramanujachary, K. V.; Collins, B. T.; Greenblatt, M.; McNally, P.; McCaroll, W. H. *Solid State Ionics* **1986**, *22*, 105. (e) Matsuda, Y.; Onoda, M.; Sato, M. *Physica. B+C*: **1986**, *143B+C*, 243.

(13) Hoffmann, R. *J. Chem. Phys.* **1963**, *39*, 1397.

0002-7863/87/1509-6308$01.50/0

were taken from ref 6f. In what follows, we first examine the structural characteristics of $K_{0.9}Mo_6O_{17}$ and then discuss its d-block band electronic structure and its associated Fermi surfaces. Finally, we analyze the essential features of the calculated d-block bands from the viewpoint of orbital interactions.

Crystal Structure

It is convenient to describe the crystal structure of the Mo_6O_{17} layer in $K_{0.9}Mo_6O_{17}$ in terms of the "building unit" Mo_4O_{21} (**1**),

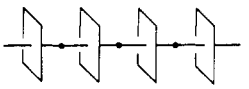

1

which is constructed from four MoO_6 octahedra by sharing the axial oxygen atoms. Shown in **2a** is a schematic representation of the hexagonal layer Mo_4O_{15} ($a = b \neq c$, $\alpha = \beta = 90°$, $\gamma = 120°$) constructed from the Mo_4O_{21} chains: Along the crystallographic *b* axis, every adjacent pair of Mo_4O_{21} chains share the equatorial oxygen atoms of three MoO_6 octahedra. Though not shown explicity, every MoO_6 octahedron of **2a** forms a zigzag chain Mo_2O_{10} (**3**), along the crystallographic *a* axis. The Mo_4O_{15} layer **2a** can alternatively be represented by **2b**, which makes it clear that the Mo_4O_{15} layer **2** consists of four sublayers of MoO_6 octahedra parallel to the *ab* plane. When the Mo_4O_{15} layer **2** is viewed along the crystallographic *c* axis (i.e., perpendicular to the layer as in the case of, for example, **6** discussed later), every three nearest-neighbor MoO_6 octahedra of its outer two sublayers form a triangle of oxygen atoms that can be used as a face of an MoO_4 tetrahedron. When all such oxygen triangles of the outer sublayers of the Mo_4O_{15} layer are capped by MoO_4 tetrahedra, one obtains the Mo_6O_{17} layer found in $K_{0.9}Mo_6O_{17}$. It is between these Mo_6O_{17} layers where the potassium cations K^+ reside.

2a

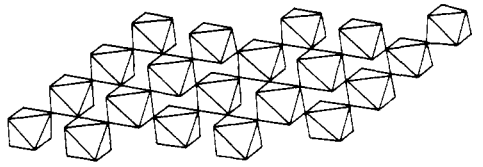

2b

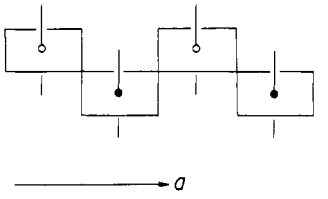

3

Thus there exist three types of Mo atoms in $K_{0.9}Mo_6O_{17}$: the Mo atoms of the MoO_4 tetrahedra (Mo_I), those of the MoO_6 octahedra in the outer two sublayers of the Mo_4O_{15} layer (Mo_{II}), and those of the MoO_6 octahedra in the inner two sublayers of the Mo_4O_{15} layer (Mo_{III}). In connection with the electrical and other physical properties of $K_{0.9}Mo_6O_{17}$, it is essential to know how the d electrons are distributed among the three different Mo atoms. Empirically, this question is answered by performing a Zachariasen analysis[14] of metal–oxygen bond lengths, in which the difference between the length r_i of a given bond *i* and its standard bond length r_0 is related to the strength s_i of that bond as follows:

$$r_i - r_0 = \alpha \ln s_i \quad (1)$$

where α is a positive constant and the s_i value means the number of electrons associated with bond *i*. Thus the sum of the s_i values for all the bonds *i* around each metal is equal to the total number of d electrons the metal lost in forming those bonds (i.e., the formal oxidation state of the metal). When the constants r_0 and α for $K_{0.9}Mo_6O_{17}$ are chosen such that the oxidation state of Mo_I becomes +6, the oxidation states of Mo_{II} and Mo_{III} are calculated to be +5.8 and +5.1, respectively.[7] In other words, the d electrons of $K_{0.9}Mo_6O_{17}$ reside primarily in the MoO_6 octahedra of Mo_{III}. Therefore, the inner two sublayers of the Mo_4O_{15} layer are expected to play an important role in determining the electronic structure of the Mo_6O_{17} layer and hence that of $K_{0.9}Mo_6O_{17}$.

The inner two sublayers of **2** are schematically shown in **4**, which has the composition of Mo_2O_9. This layer may be considered to originate from the "building unit" Mo_2O_{11}, **5a**. An alternative view of **5a** is shown in **5b**. A projection view of **5b** along the direction perpendicular to a triangular face of the MoO_6 octahedra is given by **5c**. With this representation of the Mo_2O_{11} unit, a projection view of the Mo_2O_9 layer **4** along the *c* axis is given in **6**. It is important to recognize that the Mo_2O_9 layer **6** is constructed from the Mo_2O_{10} chains **3** upon sharing the axial oxygen atoms as illustrated in **7**. Due to symmetry, there are three different ways of making Mo_2O_{10} chains in **6**: The Mo_2O_{10} chains are aligned along the *a*-, *b*-, and $(a + b)$-axis directions in **7a**, **7b**, and **7c**, respectively.

4

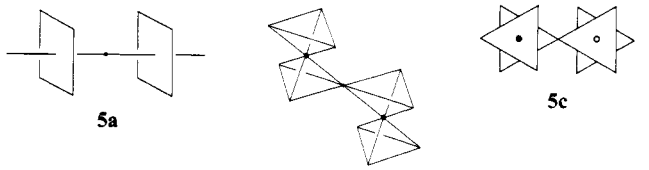

5a **5b** **5c**

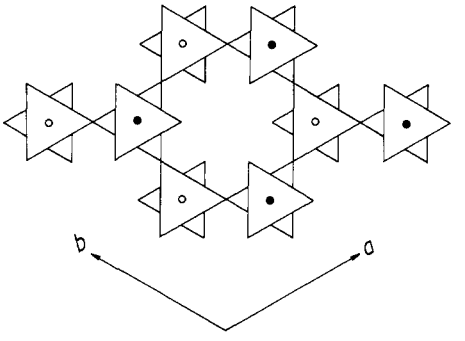

6

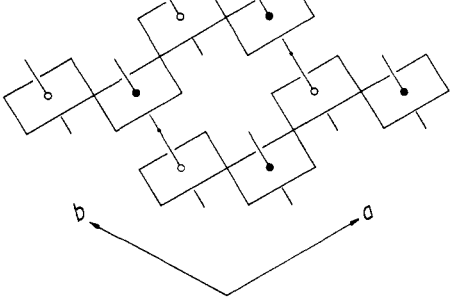

7a

(14) Zachariasen, W. H. *J. Less-Common Met.* **1978**, *62*, 1.

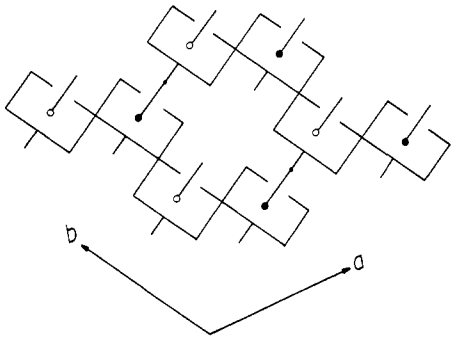

7b

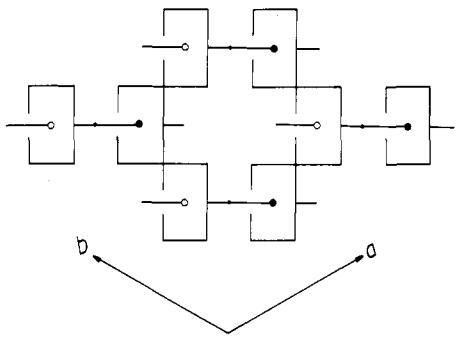

7c

Band Electronic Structure

For a 2D hexagonal lattice (i.e., $a = b$, $\gamma = 120°$) such as the Mo_2O_9 layer **6**, the Mo_4O_{15} layer **2**, or the Mo_6O_{17} layer, the first Brillouin zone of its reciprocal lattice is a regular hexagon centered at the origin Γ as shown in Figure 1.[15] In units of the reciprocal vectors a^* and b^*, the points Γ, M, K, and K′ are defined as follows: Γ = (0, 0), M = ($a^*/2$, 0), K = ($a^*/3$, $b^*/3$), and K′ = ($a^*/2$, $b^*/2$). In this section, we examine the d-block bands of the "ideal" and/or the "real" structures of the Mo_2O_9 layer and the Mo_6O_{17} layer calculated for wave vectors k along the Γ → M → K → Γ line. In our discussion, an "ideal" layer refers to one in which MoO_6 octahedra or MoO_4 tetrahedra are regular in shape, while a "real" layer refers to one in which MoO_6 octahedra or MoO_4 tetrahedra have shapes as found in $K_{0.9}Mo_6O_{17}$.

Just as the t_{2g}-block levels of an MoO_6 octahedron lie below the e_g-block levels, the t_{2g}-block bands of the Mo_2O_9 layer lie below the e_g-block bands. Figure 2 shows the t_{2g}-block bands calculated for the ideal Mo_2O_9 layer **6**, where the two bands indicated by asterisks are each doubly degenerate. Thus, the t_{2g}-block bands consist of six bands, as expected from the presence of two metal atoms in the unit cell. The t_{2g}-block bands of the real Mo_2O_9 layer are shown in Figure 3, which are very close in character to those of the ideal Mo_2O_9 layer. The MoO_6 octahedra of the real Mo_2O_9 layer are slightly distorted from a regular MoO_6 octahedron, so the degeneracy in the t_{2g}-block bands of the ideal layer is somewhat lifted by the structural change to the real layer.

Shown in Figure 4 is the bottom portion of the d-block bands calculated for the real Mo_6O_{17} layer. It is observed that the bottom three d-block bands of the Mo_6O_{17} layer are essentially identical with those of the real Mo_2O_9 layer. The bottom three d-block bands of the Mo_6O_{17} layer have the d-orbital character of primarily Mo_{III} atoms. The d-block bands of mainly Mo_I and Mo_{II} character all lie above the bottom three d-block bands. With 2.9 d electrons per $K_{0.9}Mo_6O_{17}$ (i.e., $K^+_{0.9}Mo_6O_{17}{}^{0.9-}$) or 2.9 d electrons to fill the d-block bands of Figure 4, only the bottom three bands are partially filled. This result is in agreement with the prediction of the Zachariasen analysis that the d electrons of $K_{0.9}Mo_6O_{17}$ reside primarily in the Mo_{III} atoms of the Mo_2O_9 layer.[7]

(15) Lax, M. *Symmetry Principles in Solid State and Molecular Physics*; Wiley: New York, 1974.

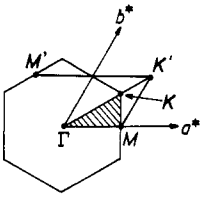

Figure 1. First Brillouin zone of a 2D hexagonal lattice.

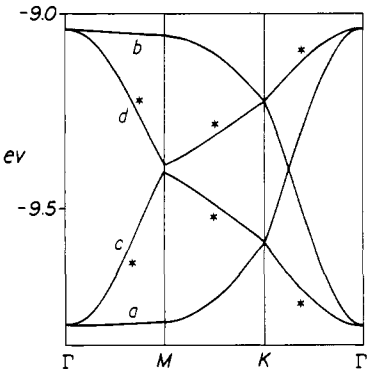

Figure 2. t_{2g} block bands of the ideal Mo_2O_9 layer.

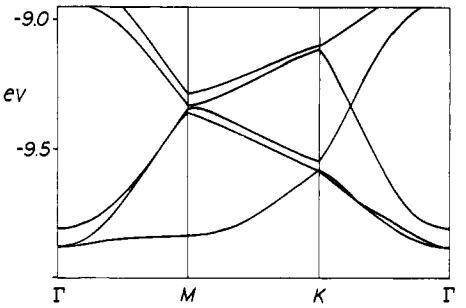

Figure 3. t_{2g} block bands of the real Mo_2O_9 layer.

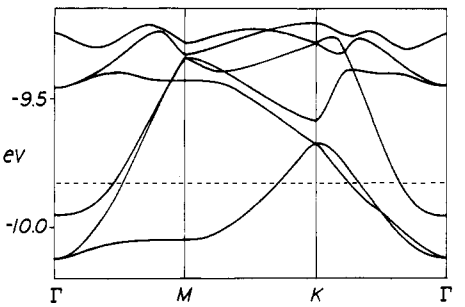

Figure 4. Bottom portion of the d-block bands of the real Mo_6O_{17} layer.

For a partially filled band, a certain region of wave vectors of the Brillouin zone leads to occupied band levels, and another region to unoccupied band levels. The Fermi surface of a partially filled band is the boundary surface of wave vectors that separate the occupied wave vector region from the unoccupied wave vector region. When the Fermi level is close to the top (bottom) of a partially filled band, the unoccupied (occupied) region of wave vectors is referred to as a hole (electron) pocket. If a piece of a Fermi surface is related to another piece by a mere translation of wave vector q, the two pieces are said to be nested by q. Such a nesting is favorable for a CDW of wave vector q.

The Fermi surfaces calculated for the three partially filled bands of the Mo_6O_{17} layer are shown in Figure 5, where the shaded and unshaded regions signify the occupied and unoccupied regions, respectively. As shown in parts a and c of Figure 5, the first and the third d-block bands (from the bottom) of the Mo_6O_{17} layer give hole pockets around K and an electron pocket around Γ, respectively. The Fermi surfaces of these two bands do not have good nesting. The second d-block band (from the bottom) of the

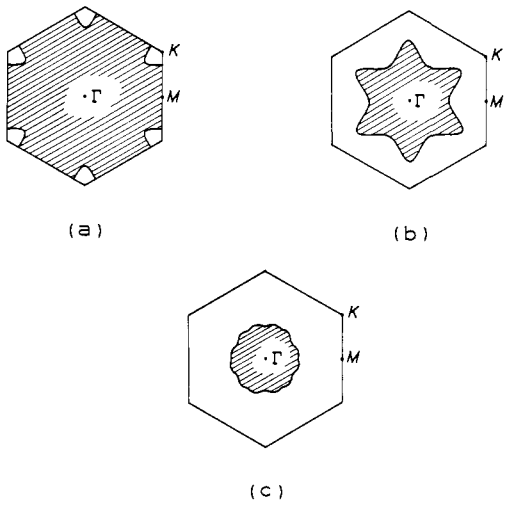

Figure 5. Fermi surfaces for the first, second, and third d-block bands (from the bottom) of the Mo_6O_{17} layer in (a), (b), and (c), respectively.

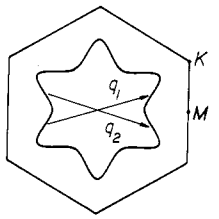

Figure 6. Two pairs of nested pieces of the Fermi surface associated with the second d-block band of the Mo_6O_{17} layer.

Mo_6O_{17} layer leads to the Fermi surface in Figure 5b, which gives rise to six pairs of nested pieces as illustrated for two of them in Figure 6. In our calculations, the a^* component of the nesting vectors q_1 and q_2 is very close to $a^*/2$. The vectors q_1 and q_2 cancel out their b^* components and therefore are responsible for the superlattice spot at $q_a = (a^*/2, 0, 0)$ in $K_{0.9}Mo_6O_{17}$. In a similar manner, the remaining four nesting vectors account for the superlattice spots at $q_b = (0, b^*/2, 0)$ and $q_{a+b} = (a^*/2, b^*/2, 0)$.

All three Fermi surfaces of the Mo_6O_{17} layer are closed, so that the potassium purple bronze is a 2D metal. The CDW of $K_{0.9}Mo_6O_{17}$ that sets in at 120 K is caused by the nesting of the Fermi surface resulting from the second d-block band. This CDW does not affect the Fermi surfaces associated with the first and third d-block bands. Consequently, $K_{0.9}Mo_6O_{17}$ remains a 2D metal below 120 K, and its carriers below 120 K consist of electrons and holes as expected from Figure 5a,c, respectively. All of these results are in good agreement with experiment.[8,9]

t_{2g}-Block Bands of the Ideal Mo_2O_9 Layer

As discussed in the previous section, the bottom three d-block bands of the Mo_6O_{17} layer are responsible for the 2D metallic, CDW, and other physical properties of $K_{0.9}Mo_6O_{17}$. In understanding these properties, it is crucial to examine how those bands come about. In this section, we probe this question by analyzing the nature of the t_{2g}-block bands of the ideal Mo_2O_9 layer since the bottom portion of these bands is essentially similar to the three partially filled bands of the Mo_6O_{17} layer and since the high symmetry of the ideal Mo_2O_9 layer makes our analysis simple.

A. Metal–Ligand Interactions. The three t_{2g} levels of an MoO_6 octahedron are shown in **8**, where small antibonding contributions from the ligand oxygen orbitals are omitted for simplicity. For

8

our discussion, it is crucial to recall that in d-block levels of most transition-metal compounds, the ligand orbitals combine out-of-phase (i.e., in an antibonding way) with the metal d-orbitals. Therefore, the energy of a d-block level is raised or lowered when the ligand orbital contribution increases or decreases, respectively.

In the Mo_2O_9 layer, the Mo atoms interact with one another via Mo–O–Mo bridges. As shown in **7**, Mo_2O_9 can be regarded as being derived from the Mo_2O_{10} chains **3** upon sharing their axial oxygen atoms. Thus there are two types of Mo–O–Mo bridges in the Mo_2O_9 layer: One is within each Mo_2O_{10} chain, and the other is between adjacent Mo_2O_{10} chains. Along the intra- and interchain Mo–O–Mo bridges, the p orbitals of the bridging oxygen may interact with the adjacent metal d orbitals as depicted in **9** and **10**, respectively. In **9a**, **10a**, or **10b**, all the interacting orbitals are contained in a plane, while this is not the case in **9b** or **9c**. Hence, the π-type overlap present in **9a**, **10a**, or **10b** is greater than that in **9b** or **9c**.

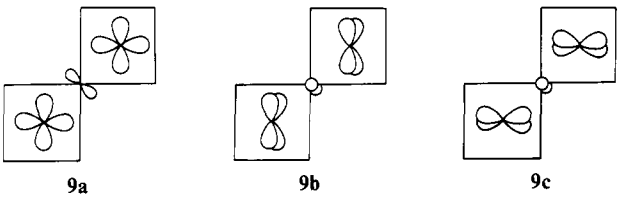

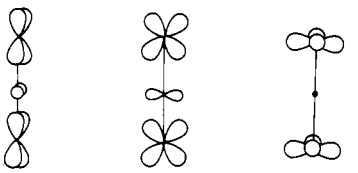

For the bridging oxygen p orbitals to mix with the adjacent metal d orbitals in **9** and **10**, the two metal orbitals of an Mo–O–Mo bridge must have an in-phase combination (e.g., see the orbital ϕ_1^+ in **12**). Otherwise, the bridging oxygen p orbital cannot mix with the metal d orbitals (e.g., see ϕ_1^- in **12**).[17] In **10c**, the metal orbitals have a δ-type interaction, and thus none of the bridging oxygen orbitals can mix with the metal d orbitals (e.g., see **15**).

B. Band Dispersion. Point K′ in Figure 1 is equivalent to M′ = $(-a^*/2, b^*/2)$, since M′ differs from K′ by an integral multiple of the reciprocal vector;[15] i.e., M′ = K′ − $(a^*, 0)$. By symmetry, M′ is equivalent to M, so that the K → M line of the Brillouin is equivalent to the K → K′ line. Thus, in our discussion, the Γ → K → M line can be replaced by the Γ → K′ line. Then essential features of the d-block bands of the ideal Mo_2O_9 layer in Figure 2 are summarized as follows: (a) The nondegenerate bands a and b are flat along Γ → M but strongly dispersive along Γ → K′. In addition, the two bands cross each other along Γ → K′. (b) The doubly degenerate bands c and d are both equally dispersive along Γ → M and along Γ → K′, the extent of the dispersion being half that of the bands a and b along Γ → K′. In the following we examine these trends in terms of orbital interaction analysis.[17]

1. Bands a and b. On going from Γ to M, the phases between nearest-neighbor unit cell orbitals remain in-phase in one direction (e.g., b axis in **7b**) but change from in-phase to out-of-phase in the other direction (e.g., a axis in **7a**).[17] To simplify our representation of band orbitals, the "building unit" Mo_2O_{11}, **11**, of the Mo_2O_{12} chain **3** may be represented by **12**. On the basis of the Mo_2O_9 layer **7b**, the bands a and b at Γ = (0, 0) are given by the orbitals **13a** and **13b**, respectively. And the bands a and b at M = $(a^*/2, 0)$ are given by the orbitals **14a** and **14b**, respectively. Note that **13a** and **14a** are derived from the unit cell orbitals ϕ_1^- of **12**, while **13b** and **14b** are derived from the unit cell orbitals

(16) Albright, T. A.; Burdett, J. K.; Whangbo, M.-H. *Orbital Interactions in Chemistry*; Wiley: New York, 1985; Chapter 15.

(17) Whangbo, M.-H. *Crystal Structures and Properties of Materials with Quasi One Dimensional Structures*; Rouxel, J., Ed.; Reidel: Dordrecht, The Netherlands, 1986; p 27.

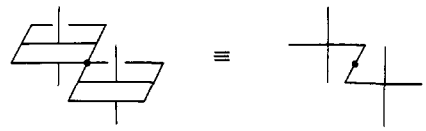

11

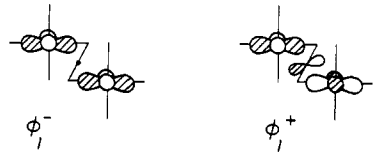

12

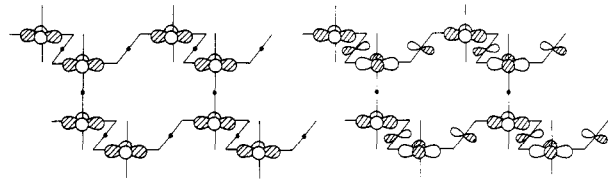

13a 13b

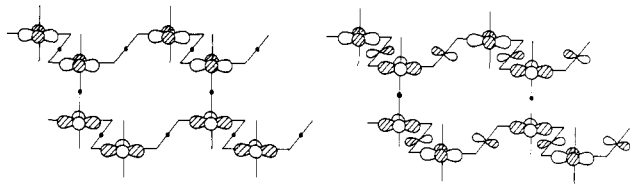

14a 14b

ϕ_1^+ of **12**. As summarized in Table I, the oxygen orbitals of the interchain Mo–O–Mo bridges do not contribute to **13** and **14**. Those of the intrachain Mo–O–Mo bridges do not contribute to **13a** and **14a**, but they do to **13b** and **14b**, thereby raising the energies of **13b** and **14b** with respect to those of **13a** and **14a**. Since the chain orbitals do not overlap significantly across the interchain Mo–O–Mo bridges, **13a** and **14a** are nearly the same in energy, and so are **13b** and **14b**.

On going from Γ to K′, the phases between nearest-neighbor unit cell orbitals change from in-phase to out-of-phase in both the *a*- and *b*-axis directions.[17] The Mo_2O_9 layer **7c** has the unit cell orbitals ϕ_2^+ and ϕ_2^- shown in **15**. The band orbitals resulting

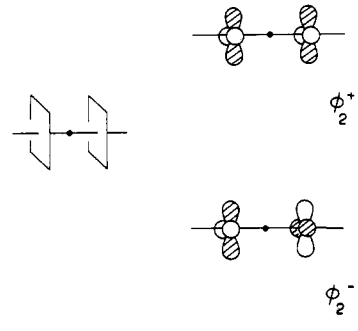

15

from ϕ_2^+ and ϕ_2^- at Γ are given by **16a** and **16b**, respectively, and those at K′ by **17a** and **17b**, respectively. As can be seen from the p-orbital contributions of the bridging oxygens, summarized in Table I, **16a** is lower in energy than **16b**, but **17a** is higher in energy than **17b**. With respect to the twofold rotation around

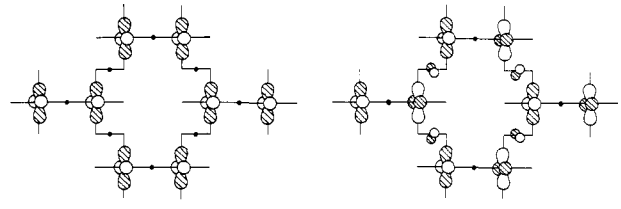

16a 16b

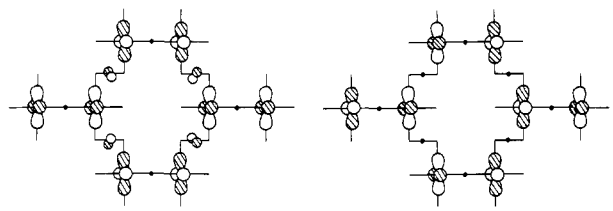

17a 17b

the $(a + b)$ axis of **7c**, **16a** and **17a** are symmetric, but **16b** and **17b** are antisymmetric. Therefore, on going from Γ to K′, **16a** and **16b** are correlated to **17a** and **17b**, respectively, and thus the two correlation curves (i.e., the bands a and b) cross each other. This explains why the bands a and b are highly dispersive along Γ → K′.

Given the translational symmetry of the Mo_2O_9 layer, **16a** and **16b** are identical with **13a** and **13b**, respectively, while **17a** and **17b** are identical with **14b** and **14a**, respectively. The latter observation is particularly interesting in that the band orbitals at M (derived from the layer representation **7b**) are identical with those at K′ (derived from the layer representation **7c**). From the viewpoint of band orbitals, this is why the M and K′ points are equivalent for a hexagonal lattice.

2. Bands c and d. On the basis of the Mo_2O_9 layer **7b**, we now examine the degenerate bands c and d along Γ → M, which are derived from the unit cell orbitals ϕ_3^+ and ϕ_3^- in **18** and ϕ_4^+ and ϕ_4^- in **19**. Since the set of ϕ_4^+ and ϕ_4^- leads to the same results

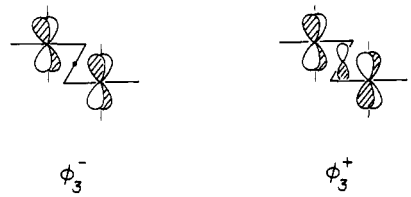

18

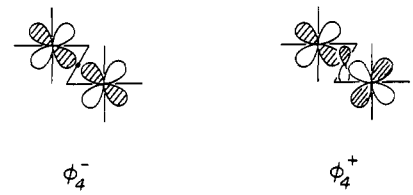

19

as does that of ϕ_3^+ and ϕ_3^-, it is sufficient to consider only the band orbitals arising from the latter.

Bands c and d at Γ are represented by **20a** and **20b**, respectively, and those at M by **21a** and **21b**, respectively. The contributions of the oxygen p orbitals of the Mo–O–Mo bridges in those band orbitals are summarized in Table I. As discussed already, the

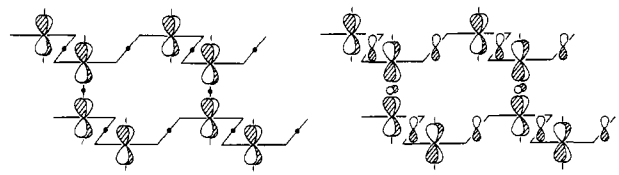

20a 20b

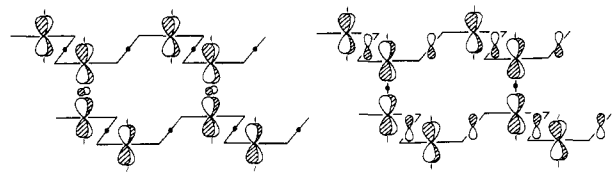

21a 21b

metal–ligand π overlap in **9b** or **9c** is weaker than that in **9a**, **10a**, or **10b**. In Table I, the stronger and weaker π overlaps are

Table I. Antibonding Contributions of the Oxygen p Orbitals of Mo–O–Mo Bridges in the t_{2g} Block Band Orbitals of the Mo_2O_9 Layer[a]

band orbital	wave vector	unit cell orbital	intrachain: within a unit cell	intrachain: between nearest-neighbor unit cells	interchain
13a	Γ	ϕ_1^-	N	N	N
13b	Γ	ϕ_1^+	Y	Y	N
14a	M	ϕ_1^-	N	N	N
14b	M	ϕ_1^+	Y	Y	N
16a	Γ	ϕ_2^+	N	N	N
16b	Γ	ϕ_2^-	Y	Y	N
17a	K′	ϕ_2^+	Y	Y	N
17b	K′	ϕ_2^-	N	N	N
20a	Γ	ϕ_3^-	N	N	N
20b	Γ	ϕ_3^+	y	y	Y
21a	M	ϕ_3^-	N	N	Y
21b	M	ϕ_3^+	y	y	N

[a] The presence of the antibonding contribution is indicated by the symbols Y or y, and the absence of it by the symbol N. The symbols Y and y refer to the stronger and the weaker antibonding contributions discussed in connection with **9** and **10**.

indicated by the symbols Y and y, respectively. **20a** has no oxygen p-orbital contribution from the Mo–O–Mo bridges and thus has the same energy as **13a**. **20b** has oxygen p-orbital contribution from all the intra- and interchain Mo–O–Mo bridges, unlike **13b**, which has oxygen p-orbital contribution only from the intrachain Mo–O–Mo bridges. Nevertheless, **20b** is degenerate with **13b** since the sum of two weak antibonding p-orbital contributions per unit cell is equivalent to one strong antibonding p-orbital contribution per unit cell. **21a** has one strong antibonding p-orbital contribution per unit cell, while **21b** has two weak antibonding p-orbital contributions per unit cell. Consequently, **21a** and **21b** are nearly degenerate, and their energies lie at the midpoint between **20a** and **20b**. This explains why bands c and d are dispersive along Γ → M and why their dispersion is half as strong as that of bands a and b along Γ → K′. In a similar way, the Mo_2O_9 layer **7c** can also be employed to show that bands c and d are equally dispersive along Γ → K′, and their dispersion is half as strong as that of bands a and b along Γ → K′.

Concluding Remarks

Our tight-binding band calculations performed on a single Mo_6O_{17} layer show the presence of three partially filled d-block bands. In agreement with the Zachariasen analysis,[7] those bands are essentially derived from the t_{2g} levels of the MoO_6 octahedra belonging to the innermost two sublayers of Mo_6O_{17}. Between adjacent Mo_6O_{17} layers, therefore, there is practically no overlap as far as the partially filled d-block bands are concerned. Thus our conclusions based upon a single Mo_6O_{17} layer are valid in discussing the electronic properties of $K_{0.9}Mo_6O_{17}$, as supported by the excellent agreement with experiment: The Fermi surfaces of the three partially filled bands show that $K_{0.9}Mo_6O_{17}$ is a 2D metal, its CDW at 120 K results from the nesting of one of the three Fermi surfaces, and the remaining two provide electron and hole carriers below 120 K. These conclusions are also valid for $Na_{0.9}Mo_6O_{17}$ and $TlMo_6O_{17}$, which are isostructural with $K_{0.9}Mo_6O_{17}$. However, we note that the sizes of the hole and electron pockets of the first and third Fermi surfaces (Figures 5a,c, respectively) are not so small (about $^1/_{18}$ and $^1/_6$ of the Brillouin zone, respectively) as suggested by the Shubnikov–de Haas study[2d] on $K_{0.9}Mo_6O_{17}$. A further experimental study is necessary. Finally, our orbital interaction analysis for the t_{2g}-block bands of the innermost two sublayers of Mo_6O_{17} shows that their essential dispersion characteristics are simply governed by whether or not the orbitals of bridging oxygen atoms can mix with the molybdenum t_{2g} orbitals.

Acknowledgment. This work was supported by NATO, Scientific Affairs Division, and also by DOE, Office of Basic Sciences, Division of Materials Sciences, under Grant DE-FG05-86-ER45259. We express our appreciation for computing time on the ER-Cray X-MP computer, made available by the DOE. We thank E. Benvas and C. Escribe-Filippini for helpful previous speculations on the Fermi surface of $K_{0.9}Mo_6O_{17}$, and Prof. M. Greenblatt for reprints and preprints.

The Variable-Temperature ESR Characterization of the Fluxional d^9 Complex Bis(1,2-bis(diphenylphosphino)ethane)rhodium(0), $Rh(dppe)_2^0$

Karl T. Mueller, Amanda J. Kunin, Stephen Greiner, Thomas Henderson, Robert W. Kreilick,* and Richard Eisenberg*

Contribution from the Department of Chemistry, University of Rochester, Rochester, New York 14627. *Received February 2, 1987*

Abstract: A variable-temperature ESR study of the paramagnetic complex $Rh(dppe)_2^0$ has been performed. The complex is found to be fluxional on the ESR time scale. At 270 K the ESR spectrum of the complex in toluene consists of a symmetric five-line pattern with $\langle A \rangle_P$ of 52 G. Upon cooling, an alternating line width effect is seen, and the spectrum changes to a pattern showing coupling to two different pairs of P donors with hyperfine couplings of 37.5 and 65 G. Analysis of the dynamic behavior leads to activation parameters $\Delta H^\ddagger$ and $\Delta S^\ddagger$ of 3.54 kcal/mol and −4.6 cal/(mol K), respectively, for the exchange process. Possible mechanisms for the exchange are pairwise lengthening and shortening of the Rh–P bonds and angular distortion of the complex to a species of C_2 symmetry. A bimolecular equilibrium is also observed by a significant decrease in the intensity of the ESR signal as the temperature is lowered. The ΔH and ΔS values for this equilibrium are −13.4 kcal/mol and −49.8 cal/(mol K), respectively, consistent with either a dimerization or the formation of an intimate ion pair, $[Rh(dppe)_2]^+[Rh(dppe)_2]^-$, for this sterically crowded system. The complex $Rh(dppe)_2^0$ is also found to react with H_2 at room temperature to form the known hydride complex $RhH(dppe)_2$.

The fluxionality of inorganic and organometallic compounds has been vigorously studied during the last two decades.[1] In general, this type of dynamic behavior in solution has been followed by variable-temperature NMR investigation from which rate

0002-7863/87/1509-6313$01.50/0